A&A 524, A26 (2010)
DOI: 10.1051/0004-6361/200913724

Astronomy & Astrophysics

The model constraints from the observed trends for the quasi-periodic oscillation in RE J1034+396

B. Czerny[1], P. Lachowicz[2], M. Dovčiak[3], V. Karas[3], T. Pecháček[3], and T. K. Das[4]

[1] Nicolaus Copernicus Astronomical Center, Polish Academy of Sciences, ul. Bartycka 18, 00-716 Warszawa, Poland
e-mail: bcz@camk.edu.pl
[2] Centre for Wavelets, Approximation and Information Processing, Temasek Laboratories at National University of Singapore, 5A Engineering Drive 1, #09-02, 117411, Singapore
e-mail: pawel@ieee.org
[3] Astronomical Institute, Academy of Sciences, Boční II 1401, 14131 Prague, Czech Republic
[4] Harish Chandra Research Institute, Allahabad 211019, India

Received 24 November 2009 / Accepted 12 September 2010

ABSTRACT

We analyze the time variability of the X-ray emission of RE J1034+396 – an active galactic nucleus with the first firm detection of a quasi-periodic oscillations (QPO). Based on the results of a wavelet analysis, we find a drift in the QPO central frequency. The change in the QPO frequency correlates with the change in the X-ray flux with a short time delay. The data specifically suggest a linear dependence between the QPO period and the flux, and this gives important constraints on the QPO models. In particular, it excludes explanation in terms of the orbiting hot spot model close to a black hole. Linear structures such as shocks, spiral waves, or very distant flares are favored.

Key words. accretion, accretion disks – galaxies: active – galaxies: individual: RE J1034+396

1. Introduction

Accretion onto black holes is a non-stationary process. Strong variability is seen in the X-ray emission of both active galactic nuclei (AGN) and galactic black holes (GBH). This variability is mostly aperiodic, but quasi-periodic modulations occasionally appear (van der Klis 1989). The quasi-periodic oscillation (QPO) phenomenon is well known in GBH where the frequency can be as high as the orbital frequency in the inner disk. Recently the QPO appearance has been reported to occur in a bright Seyfert 1 galaxy, RE J1034+396 (Gierliński et al. 2008, hereafter G08) and BL Lacertae object PKS 2155−304 (Lachowicz et al. 2009). The significance of the signal in RE J1034+396 ($f_0 \simeq 2.6 \times 10^{-4}$ Hz, period $P_0 \simeq 3733$ s) is very high, ($>3\sigma$) as determined by G08 using Vaughan's (2005) test. The result was recently confirmed by Vaughan (2010) with a Bayesian approach (although with slightly lower confidence). The existence of this QPO was used to constrain the properties of the warm absorber in this source (Maitra & Miller 2010).

Despite a number of scenarios proposed in the literature, neither the origin of stochastic variability nor the QPO phenomenon have been well understood (for reviews see e.g. van der Klis 2006; McClintock & Remillard 2006; Done et al. 2007). The standard variability studies rely on the Fourier analysis and the discussion of the time-averaged power spectrum (Feigelson & Babu 1992). For the GBH the time dependence of the QPO frequency has also been studied, but the time bins were always set long in comparison to the disk Keplerian timescale because the latter is on the order of milliseconds for GBH. In AGN the Keplerian time-scale is by a factor of $\sim 10^6$ longer, so the discovery of QPOs in AGNs opens new possibilities for the investigation of accreting black holes.

Similar to Fourier spectra methods, the wavelet analysis provides fast linear operations on data vectors. Unlike the Fourier transform, the base functions of wavelets are localized, and this brings new opportunities to the data analysis.

The wavelet analysis can be particularly useful in the exploration of the QPO phenomenon (e.g. Scargle et al. 1993; Lachowicz & Czerny 2005; Espaillat et al. 2008; Lachowicz & Done 2010). In this paper we construct for the the first time a wavelet map for RE J1034+396 data when the source showed the QPO activity. We find the QPO period to change in a time-frequency (or, equivalently, time-period) plane and we investigate the properties of this pattern. Based on the wavelet results we discuss possible constraints on the physical origin of the QPO in RE J1034+396.

2. Wavelet analysis of RE J1034+396 light curve

The source RE J1034+396 was observed by *XMM-Newton* satellite on 2007 May 31, and the resulting X-ray light curve analysis was reported in G08. Using the same procedure, we extract the source light curve in the 0.3−10 keV energy band, which covers 8.5×10^4 s of continuous observations sampled evenly every $\Delta t = 100$ s. We use the wavelet analysis codes of Torrence & Compo (1998) similarly as we did in Lachowicz & Czerny (2005). Morlet wavelet is adopted, with the standard assumption $2\pi\nu_o = 6$. We limit the scale range to the region of the expected QPO signal. The result is presented in Fig. 1 together with corresponding light curve.

The wavelet map confirms the presence of the QPO in the source at the period $P_0 \simeq 3733$ s through a range of peaks. In order to assign the confidence levels to those peaks we have performed Monte Carlo simulations. We adopted the underlying

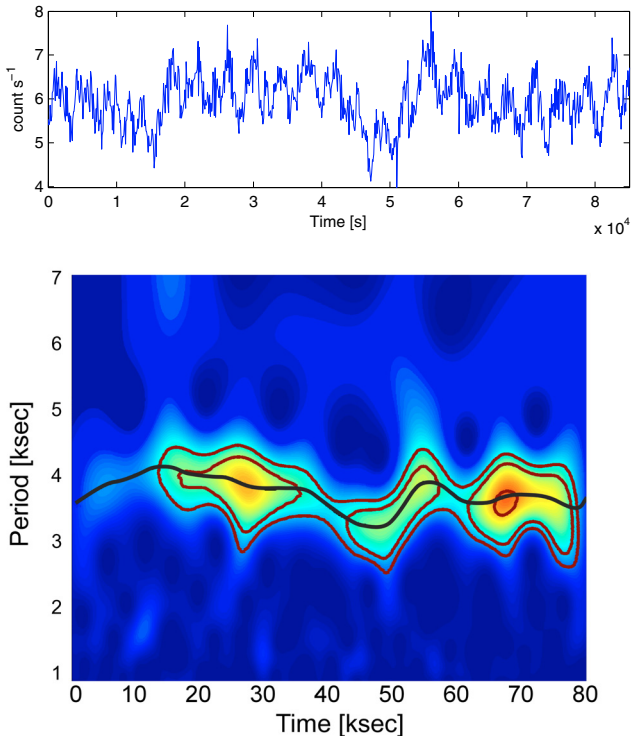

Fig. 1. (*upper*) X-ray light curve of RE J1034+396, and *(bottom)* the corresponding wavelet map. The increasing values of wavelet power are denoted by gradual changes of the colours, i.e. from deep blue, through green and yellow to red. The confidence contours of 90%, 95%, and 99% are marked, and they are shifted with respect to the color levels (see text for the discussion). A solid black line traces the the QPO period.

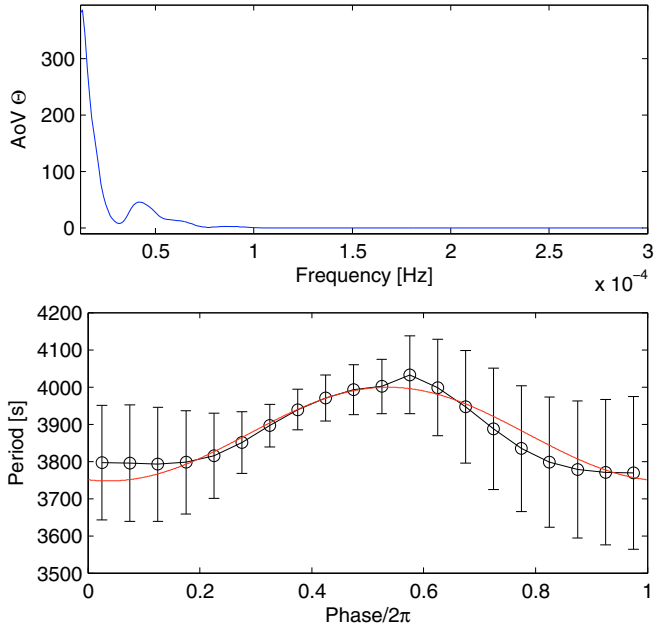

Fig. 2. (*upper*) AoV periodogram for a QPO period indicating additional periodicity at 24 008 s. *(bottom)* The QPO period curve folded with a period of 24 008 s. Although the presence of that additional period would be interesting, its formal significance is very low.

broadband power spectrum in the form of a broken power law, with the normalization and the high-frequency slope 1.35 determined by G08 for this observation of the source, and we assumed the frequency break at 10^{-5} Hz, in consistency with the data.

The simulated lightcurves were created using the algorithm of Timmer & König (1995), of the duration and timestep consistent with the observed lightcurve. We created 7500 lightcurves and the corresponding wavelet maps, and built the statistics for each of the scales in the discussed range. This allowed us to assign significance levels for each wavelet scale independently, which is important in the lightcurves with underlying red noise background. The average wavelet values rise toward longer periods, as does the power density spectrum, and this drift causes the observed misalignment between the colors on the map (referring to absolute values) and confidence levels in Fig. 1.

The significant regions are within a period range of 3000–4500 s, but they form a complex pattern. We see some very high amplitude peaks as well as indications of the period change. The QPO signal is relatively weak at the beginning of the data, as noticed by G08, who divided the lightcurve into two parts: Segment 1 to 2×10^4 s and Segment 2 above that time. In Segment 2 the QPO detection is almost always above the 90 percent confidence.

We thus investigate the wavelet map in greater detail. For every time step of Δt we fit the intensity peaks in the wavelet map with a Gaussian profile that allows us to determine the best fit of the QPO period and the wavelet amplitude at the peak. We denote this line with a black solid line in the wavelet map (see Fig. 1, lower panel). The errors of the peak position were estimated at the basis of the largest error in the flux determination (0.26 cts s^{-1}). The peak position errors are large in the Segment 1, but they are well constrained in Segment 2.

The QPO period marked by the peak positions seems to follow a complex pattern in the time-period plane. The changes in the frequency are significant: the χ^2 fit to this pattern assuming constant period value gave unacceptable results (reduced $\chi^2 = 6.9$).

In order to find out whether any additional periodicity is present in the system, we analyzed a temporal variability of the QPO period. We employ the Analysis of Variance (AoV) method of Schwarzenberg-Czerny (1996) and calculate the AoV periodogram for the QPO period curve. We allow for an oversampling by a factor of 5 in the periodogram because otherwise the resolution is insufficient for a tentative period detection at the lowest frequencies. The periodogram analysis indicates a timescale of ~24 008 s (see Fig. 2, upper panel). After Lachowicz et al. (2006) we determine its significance, $P_1 = 0.5982$, to be low, i.e. at the 40.18% of confidence ($\Theta = 46.1$, $n = 851$, $n_{\rm corr} = 70.91$, $N = 1$). The actual value may be even lower because the data points obtained from the wavelet map are partially correlated (Maraun & Kurths 2004). The folded QPO period curve is shown in bottom panel of Fig. 2. It displays approximately a sinusoidal trend, but with very large errors. We also checked for the presence of this putative period directly in the X-ray lightcurve. The folded X-ray light curve (starting at 2.5×10^4 s; Segment 2 in notation of G08) with the 24 ks period is shown in Fig. 3). Again, a pattern seems to be present there, but the formal significance of the 24 008 s periodicity in the X-ray light curve estimated using the Vaughan (2005) test is low because of the fairly high red-noise level.

Concluding, the temporal modulation of the QPO period on the 24 ks time-scale is visible, both the period and the wavelet amplitude vary in time, and the X-ray light curve follows the pattern but the modulation cannot be considered as firmly periodic for the present data. However, this outcome suggests that

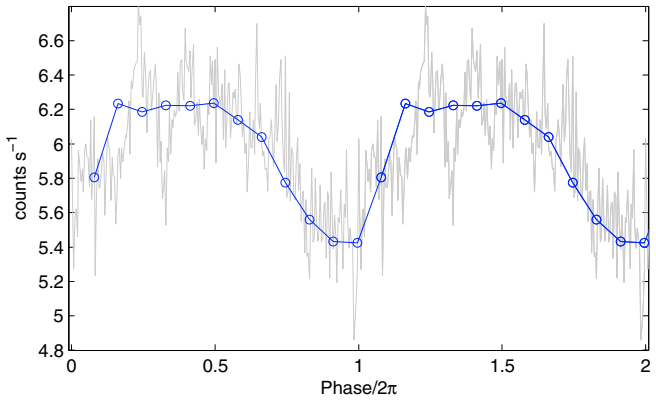

Fig. 3. Folded light curve with a period of 24 ks (blue line), derived for the second part of the light curve from Fig. 1, i.e from 2.5×10^4 s till the end of the data (gray line); plotted over two periods for clarity.

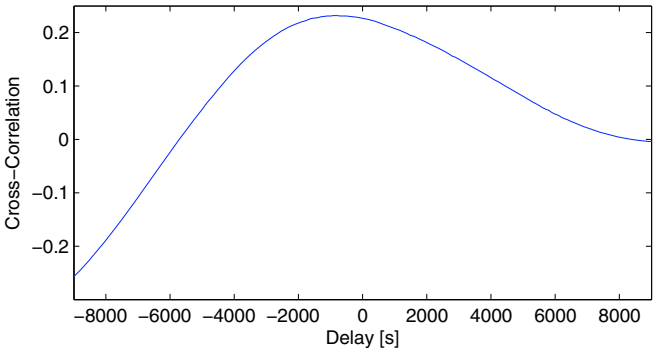

Fig. 4. Normalized cross-correlation function of the QPO period and the X-ray light curve over the whole data range. The flux change is delayed by ~900 s with respect to the change in the QPO period.

some underlying mechanism must be present and responsible for observed modulation of the QPO amplitude, the frequency and the flux. Below, we study a correlation between X-ray flux and QPO period without referring to any periodicity in their correlated behaviour.

3. Flux versus QPO period trend

The wavelet map shows a strong decrease in the marked QPO period at the time about 5×10^4 s, which is accompanied by a decrease in the X-ray flux. This motivated us to check for the overall correlation between the flux and the QPO period in the data. The cross-correlation function between the X-ray luminosity and the QPO period is shown in Fig. 4. The correlation is present, and the time delay between the curves is ~900 s, with the flux lagging behind the frequency change. The delay is by a factor 4.1 shorter than the QPO period itself. If only the second part of the data is investigated (Segment 2 in notation of G08), the measured delay is somewhat longer (1400 s).

Therefore, we made a logarithmic plot (see Fig. 5, upper panel) of the dependence of the flux on the observed QPO period allowing for a shift according to the measured delay. If the full light curve is used, with the delay of 900 s, the correlation coefficient r between the quantities is very low, 0.26, and the slope of the best-fit straight line is 0.42 ± 0.05. If only the Segment 2 is used with the delay of 1400 s, $r = 0.52$, and the slope is 1.03 ± 0.07. This means that the correlation is much more significant, and the slope is close to 1.

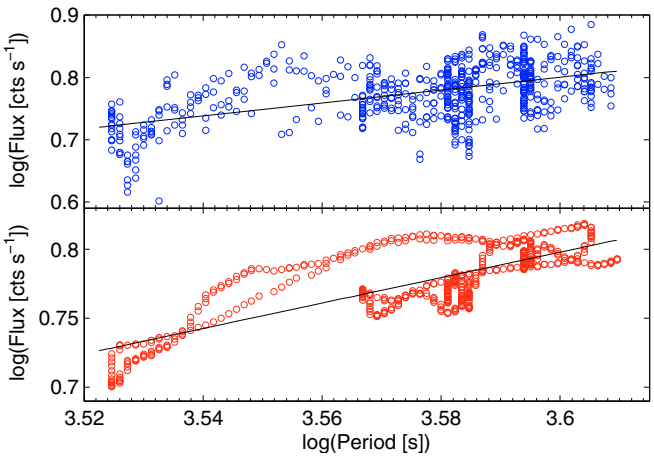

Fig. 5. *(upper)* Flux vs. QPO period relation in the Segment 2 of the data for original X-ray light curve, and (*bottom*) the smoothed light curve.

We justified the omission of Segment 1 by examining the flux–period relation for the QPO in this part of the data. Visually, there seems to be a dip in the flux at time $\sim 1.6 \times 10^4$ s accompanied by a rise rather than a fall in period, and the presence of this dip might be used as a counter-argument for positive flux-period correlation, and the significance of the QPO detection in this period (between $\sim 1.5 \times 10^4$ and $\sim 1.7 \times 10^4$ s) is relatively high (between 90 and 95% confidence level). However, in most of the Segment 1 data the significance of the QPO detection is below 90%, and in addition the dynamical range of the measured quantities (including the dip period) is lower than in the Segment 2 while the dispersion is large. As a result, there is no correlation between the flux and period in this segment alone. If all Segment 1 data points are plotted in Fig. 5, they group in the long period part of the diagram without showing an expected rise in the flux. The dip partially shows an extreme trend, with the three data points having the lowest value of the flux and the highest value of the period, but all other data points during the dip (18) overlap with the rest of the distribution, so the trend seen during this dip cannot be considered as significant. Thus, we concentrate on the result from the Segment 2 alone in our discussion below.

Since the QPO of a 3733 s period smears the correlation at the longer time-scales, we extract the short-time trend from the light curve by applying the moving average approach, with a 5000 s window function. In consequence, we obtain a smoothed curve, free from temporal high-frequency flux variability.

If we now use this long time-scale component for a whole light curve, the measured delay between the flux and the period is somewhat shorter, 700 s, the correlation coefficient is slightly higher, 0.40, and the slope remains comparable, 0.38. If only the Segment 2 data are used, i.e. when the QPO is the most prominent, the delay is slightly shorter than for a whole light curve, now 1200 s, the correlation becomes more significant ($r = 0.80$), and the slope is again close to 1 (see Fig. 5, lower panel), although a bit smaller (0.92 ± 0.03).

The results for the Segment 2 (when the QPO and the correlation are strong) for the original and the smoothed light curve are shown in Fig. 5, respectively. Both of them show similar trends, but the dispersion is clearly lower for the smoothed light curve. Straight lines show the best linear fits. This linear relation with the slope of 1 (i.e., a simple proportionality of the flux and

QPO period with an offset from zero) is an important constraint for the models of QPO itself.

Because the amplitude of the wavelet map also varies considerably, we tested for other possible correlations as well. The weak correlation between the wavelet amplitude and the QPO period was present but it was less significant than the correlation of X-ray flux vs. QPO period. The highest value of the correlation coefficient for the amplitude-period was 0.47 (lower than 0.52 for the flux-period correlation for un-smoothed flux and 0.80 for a smoothed flux; all correlations measured for Segment 2 only), and the delay was again 1400 s. The X-ray flux, whether smoothed or not, was uncorrelated with the wavelet amplitude.

4. Discussion

We performed the wavelet analysis of the XMM X-ray lightcurve of REJ 1034+396 from 2007 May 31, when the source showed a clear QPO phenomenon (G08). Other observations of this source did not show such a signal on the top of the typical red noise (Done, private communication) but this is not surprising in view of the low duty cycle for a QPO phenomenon in the Galactic black holes. The phenomenon is most likely to be an example of the high-frequency QPO, as discussed by Middleton et al. (2009) and Bian (2009).

Our analysis of the X-ray light curve of RE J1034+396 through wavelet technique indicates the dependence of the QPO peak position on time, and the change of the QPO period correlates with the X-ray flux. This correlation implies a common source of perturbation.

Qualitative study of this relation suggests a linear dependence between the flux and the QPO period. Because the trend in the QPO period is likely to be connected with the change in the size/shape of the oscillating region, we can try to constrain the geometry by estimating the rate of change of both the frequency and flux.

In the simplest dimensional analysis approach, we can assume that the local properties of the emitting region do not depend on the region size. The characteristic period is then likely to be proportional to the total size of oscillation region, while the emitted flux is expected to rise with a region volume. Therefore, within this simplest scenario we would expect flux $\propto R^3$ for a spherical region, flux $\propto R^2$ for a flat region and flux $\propto R$ for a linear emitting region. Only the last one would reproduce the observed linear relation between the flux and the oscillation period.

4.1. Oscillating and dissipating tori

The more realistic models of the QPOs are based on the computations of the tori around black holes. The proper frequencies of these tori oscillations are on the order of the Keplerian period, P, at the torus outer edge, R. Therefore, in this case $P \propto R^{3/2}$. The overall torus emissivity is likely to be related to the accretion dissipation inside this region. In a simple accretion disk approach, the dissipated energy depends mainly on the inner radius, $R_{\rm in}$, and only weakly on the outer radius R unless these two radii are very close. For the latter, the dissipation inside is roughly proportional to $(R - R_{\rm in})$. Therefore, for a moderately wide torus the significant change of the flux following the change of the period is not expected, and for a narrow ring the flux response may be arbitrarily strong. However, a linear response does not seem to be favored.

The quantitative models of the QPOs published so far do not show the connection between the average flux and the adopted outer radius required in testing the QPO mechanism according to our finding (see e.g. Schnittman & Rezzola 2006; Horak 2008).

4.2. Emission of the magnetic flare on the Keplerian orbit

Typical AGN light curves are stochastic but, occasionally, the distinct large flares have been reported either in the light curve itself (Ponti et al. 2004) or in the periodic behavior of the iron line (e.g. Iwasawa et al. 2004; Turner et al. 2002, 2006; Guainazzi 2003; Yaqoob et al. 2003; Dovčiak et al. 2004; Markowitz et al. 2006). A magnetic loop can expand or contract in length, eventually producing the linear flux-period relation required by the data.

However, in the case of the disk, this flare is likely to perform an orbital motion around a central black hole, sharing the bulk motion with the underlying accretion disk. Then the relativistic effects will also couple the flux and the period, but in the opposite direction; the Doppler boosting enhances both the flux and the frequency, so the anti-correlation between the flux and the period is expected, in contrast to what is observed. Only if the flare is very distant, or observed at a very low inclination angle, the relativistic effects will be negligible. Here, we study the required conditions with a simple model.

We assume that the intrinsic flare oscillation has a fixed frequency, f_0, and the flare is anchored in a Keplerian accretion disk. The effect of relativistic periodic change of the flare frequency and luminosity can be modeled by parametrizing the flare position radius r, measured in gravitational radius units ($R_{\rm g} = GM/c^2$), the initial phase ϕ_0, and the inclination of an observer, i with respect to the accretion disk. We approximate the flare geometry by a point-like source radiating isotropically. In the center, we assume a Schwarzschild black hole because the probable radii are large and at these distances the corrections because of the black hole spin are negligible (Murphy et al. 2009).

The flare frequency as seen by the observer can be calculated from the formula $f(t) = f_0 g(r, \phi)$, where the $g(r, \phi)$ factor is (Pecháček et al. 2006)

$$g(r,\phi) = \frac{r^{1/2}(r-3)^{1/2}}{r + \sin\phi\ \sin i\ \sqrt{[r-2+4(1+\cos\phi\sin i)^{-1}]}}\cdot \qquad (1)$$

The flare in Keplerian orbital motion has the position angle ϕ varying with time. However, the observed rate of $\phi(t)$ is not uniform because of the time delays owing to the light-travel time that photons experience from different points in the orbit. The time delay can be approximated as follows

$$t = \frac{\phi}{\Omega_{\rm K}(r)} + (r-1)(1-\cos\phi)\sin i + 2\ln\frac{1+\sin i}{1+\sin i\cos\phi}, \qquad (2)$$

where $\Omega_{\rm K}(r)$ is the Keplerian angular velocity. The flare intensity is then

$$L = L_0\ g(r,\phi)^4\left[1+\frac{1}{r}\frac{1-\sin i\ \cos\phi}{1+\sin i\ \cos\phi}\right]\cos i. \qquad (3)$$

Assuming a black hole mass $2\times10^6\ M_\odot$ we determined the fractional amplitude of a flare owing to the relativistic motion for a range of radii and inclination angles. Because the QPO itself contains about 10% of the total power of the source (Gierlinski et al. 2008), and a fractional change in the observed trend is about 5% (see Fig. 3), then a relativistic effect at the level of 20% would totally cancel the observed opposite trend and only the effect at the level about 5% may pass unnoticed. We show the lines of a constant fractional flux enhancement as functions of

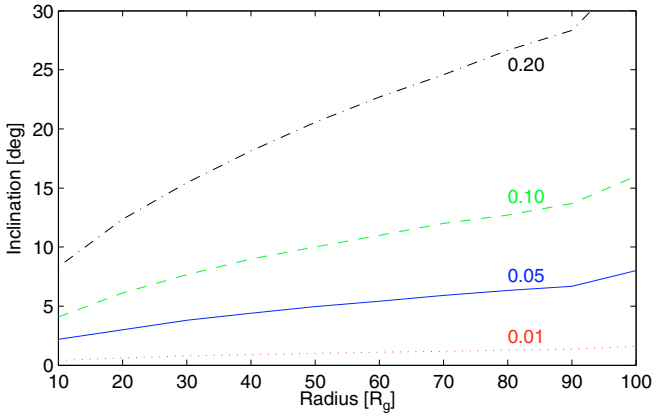

Fig. 6. Expected fractional flux enhancement anti-correlated with the QPO period for a flare in the Keplerian motion as a function of the orbital radius and the inclination angle. The flare must be located far away or the inclination must be low to ensure that this effect does not suppress the observed opposite trend. Amplitudes larger than ~0.05 (above the continuous blue line) are highly improbable, and low inclination (below 10 deg) is required for a flare model.

the flare location in Fig. 6. The blue continuous line in this plot marks acceptable range, so the disk inclination should be lower than 2–3 deg for flares close to a black hole, and inclinations up to 7–8 deg are acceptable for flares at a distance of 100 R_g. We have no observational constraints for RE J1034+396, but the inclinations of other radio quiet AGN are typically estimated to be about 30 deg.

Very distant flares, at radii much larger than 100 R_g are not excluded by this consideration. Then the relativistic effects become unimportant and the flare luminosity changes only because of its intrinsic evolution which may involve pulsations.

4.3. Shocks and spiral waves

In a series of papers (see e.g. Das et al. 2003; Mondal et al. 2009) the QPO phenomenon was modeled as caused by the oscillations of a shock that forms in a thin accretion flow. The applicability of the model is not immediate because RE J1034+396 is a disk-dominated source. However, a coronal flow may be present with properties similar to the predicted in the model without the underlying Keplerian disk. In those models, there is a relation between the outflow rate (which may be used as a proxy to luminosity) and the frequency, and this relation for low values of the entropy an angular momentum has a power-law shape, but an index of only 0.25 (Das et al. 2003, Fig. 3, upper left panel, two lowest curves). However, a better proxy for the system luminosity yields an index consistent with the observed one (Das & Czerny 2010).

Spiral waves were also suggested as a possible explanation of the QPO phenomenon, (e.g. Tagger & Varniere 2006; see also Chan et al. 2009, for a study in the context of Sgr A*) and because of their predominantly linear structure they may possibly give the requested flux-QPO period relation. The spiral wave rotates with constant angular velocity, and the average rotation speed of this pattern is likely to be considerably lower than Keplerian in the innermost part of the disk, although the matter itself is still roughly in Keplerian motion. It may reduce the strength of the relativistic effects and act against the positive correlation between the flux and frequency resulting from a slow pattern evolution. However, the quantitative modeling would be needed to see if the coherent model of the phenomenon can be found within the frame of this scenario. Simulations of the flare-like events for Sgr A* perhaps show occasional traces of the correlated change in the period and flux for a given oscillation (see Fig. 12 of Chan et al. 2009), but the results may not directly apply to REJ 1034+396.

5. Conclusions

The wavelet analysis of the X-ray light curve of RE J1034+396 allowed us to see a trend in the QPO period during a single QPO event. An increase in the QPO central period seems to be accompanied by a proportional increase in the X-ray flux.

This observation is unique because the source did not show any QPO phenomenon at another time apart from the observation analyzed by Gierlinski et al. (2008), and the claimed QPO events in other AGN are less significant (Espaillat et al. 2008; Lachowicz et al. 2009). The detection of the trend within the QPO is difficult, but the signal seems to be there. If the result indicating the proportionality between the flux and the QPO period during a single QPO event is a general property, then it implies very strong constraints on the QPO mechanism. The oscillating tori seem less likely, the linear structures are favored (shocks or spiral waves), and they should not be involved in Keplerian motion around a black hole if they are localized at a small radius, unless the viewing angle in REJ 1034+396 is exceptionally low. The models of these structures have to be further developed and they should, at some point, also explain why the oscillating hard X-ray emitting plasma responsible for QPOs (Middleton et al. 2009; van der Klis 2006; Życki et al. 2007) has to coexist with the accretion disk.

In galactic sources single QPO high-frequency events are unresolved, therefore this newly found correlation cannot be tested. However, future X-ray observations (e.g. with IXO) will bring many more light curves of AGN with a quality good enough to perform a similar analysis, even if the QPO duty cycle is relatively low, as in galactic black holes.

Acknowledgements. Wavelet software was provided by C. Torrence and G. Compo, and is available at the URL: http://atoc.colorado.edu/research/wavelets/. We thank Piotr Życki and Alex Schwarzenberg-Czerny for very helpful discussions. This work was supported in part by grant NN 203 380136. V.K. and M.D. acknowledge the Czech Science Foundation grants 205/07/0052 and 202/09/0772.

References

Bian, W. 2010, in The Starburst-AGN Connection, proceedings of the conference held 27–31 October 2008, at Shanghai Normal University, Shanghai, China, ed. Weimin Wang, Zhaoqing Yang, Zhijian Luo, & Zhu Chen (San Francisco: ASP), 2009, ASP Conf. Ser., 408, 303
Chan, C., Siming, L., Fryer, C. L., et al. 2009, ApJ, 701, 521
Das, T. K., & Czerny, B. 2010 [arXiv:1009.3615]
Das, T. K., Rao, A. R., & Vadawale, S. V. 2003, MNRAS, 343, 443
Done, C., Gierliński, M., & Kubota, A. 2007, A&ARv, 15, 1
Dovčiak, M., Bianchi, S., Guainazzi, M., Karas, V., & Matt, G. 2004, MNRAS, 350, 745
Espaillat, C., Bregman, J., Hughes, P., & Lloyd-Davies, E. 2008, ApJ, 679, 182
Feigelson, E. D., & Babu, G. J. 1992, Statistical Challenges in Modern Astronomy (Berlin: Springer)
Gierliński, M., Middleton, M., Ward, M., & Done, C. 2008, Nature, 455, 369
Guainazzi, M. 2003, A&A, 401, 903
Horák, J. 2008, A&A, 486, 1
Iwasawa, K., Miniutti, G., & Fabian, A. C. 2004, MNRAS, 355, 1073
Lachowicz, P., & Czerny, B. 2005, MNRAS, 361, 645
Lachowicz, P., & Done, C. 2010, A&A, 515, A65
Lachowicz, P., Zdziarski, A. A., Schwarzenberg-Czerny, A., Pooley, G. G., & Kitamoto, S. 2006, MNRAS, 368, 1025

Lachowicz, P., Gupta, A. C., Gaur, H., & Wiita, P. J. 2009, A&A, 506, L17
Maitra, D., & Miller, J. M. 2010, ApJ, 718, 551
Markowitz, A., Reeves, J. N., & Braito, V. 2006, ApJ, 646, 783
Maraun, D., & Kurths, J. 2004, Cross Wavelet Analysis. Significance Testing and Pitfalls, Nonlin. Proc. Geoph., 11(4), 505
McClintock, J. E., & Remillard, R. A. 2006, in Compact stellar X-ray sources, ed. W. Lewin, & M. van der Klis, Cambridge University Series (Cambridge University Press), 39
Middleton, M., Done, C., Ward, M., Gierliński, M., & Schurch N. 2009, MNRAS, 394, 250
Mondal, S., Basu, P., & Chakrabarti, S. K. 2009, MNRAS, 396, 1038
Murphy, K. D., Yaqoob, T., Karas, V., & Dovčiak, M. 2009, ApJ, 701, 635
Pecháček, T., Dovčiak, M., & Karas, V. 2006, AN, 327, 957
Ponti, G., Cappi, M., Dadina, M., & Malaguti, G. 2004, A&A, 417, 451
Scargle, J. D., Steiman-Cameron, T., Young, K., et al. 1993, ApJ, 411, L91
Schnittman, J. D., & Rezzola, L. 2006, ApJ, 637, L113
Schwarzenberg-Czerny, A. 1996, ApJ, 460, L107
Soria, R., & Puchnarewicz, E. M. 2002, MNRAS, 329, 456
Tagger, M., & Varniere, P. 2006, ApJ, 652, 1457
Timmer, J., & König, M. 1995, A&A, 300, 707
Torrence, C., & Compo, G. P. 1998, Bull. Am. Meteorolog. Soc., 79, 61
Turner, T. J., Mushotzky, R. F., Yaqoob, T., et al. 2002, ApJ, 574, L123
Turner, T. J., Miller, L., George, I. M., & Reeves, J. N. 2006, A&A, 445, 59
van der Klis, M. 1989, ARA&A, 27, 517
van der Klis, M. 2006, in Compact stellar X-ray sources, ed. W. Lewin, & M. van der Klis, Cambridge University Series (Cambridge University Press), 39
Vaughan, S. 2005, A&A, 356, 524
Vaughan, S. 2010, MNRAS, 402, 307
Yaqoob, T., George, I. M., Kallman, T. R., et al. 2003, ApJ, 596, 85
Życki, P. T., Niedzwiecki, A., & Sobolewska, M. A. 2007, MNRAS, 379, 123